HYSTERESIS MODELING IN MAGNETOSTRICTIVE MATERIALS VIA PREISACH OPERATORS [1]

R.C. Smith
Department of Mathematics
Iowa State University
Ames, IA 50011
rsmith@iastate.edu

Abstract

A phenomenological characterization of hysteresis in magnetostrictive materials is presented. Such hysteresis is due to both the driving magnetic fields and stress relations within the material and is significant throughout most of the drive range of magnetostrictive transducers. An accurate characterization of the hysteresis and material nonlinearities is necessary to fully utilize the actuator/sensor capabilities of the magnetostrictive materials. Such a characterization is made here in the context of generalized Preisach operators. This yields a framework amenable to proving the well-posedness of structural models that incorporate the magnetostrictive transducers. It also provides a natural setting in which to develop practical approximation techniques. An example illustrating this framework in the context of a Timoshenko beam model is presented.

[1]This research was supported in part by the National Aeronautics and Space Administration under NASA Contract Number NAS1-19480 while the author was a visiting scientist at the Institute for Computer Applications in Science and Engineering (ICASE), NASA Langley Research Center, Hampton, VA 23681. Additional support was also provided by NASA grant NAG-1-1600.

1 Introduction

Important members in the class of smart materials currently employed in control applications are magnetostrictive materials. The phenomenon of magnetostriction is defined as the strain which results when a magnetic material is subjected to a magnetic field. While this phenomenon occurs in most ferromagnetic materials, only in recently developed rare-earth materials are the strains and forces sufficiently large to facilitate their use in actuators and sensors. This has led to the use of magnetostrictive materials as ultrasonic transducers, positioners, sonar projectors (500-2000 Hz) and isolators (5-60 Hz). They are also being considered as actuators for controlling vibrations in thick structures and in heavy rotating components such as milling machine bits (further details regarding applications in which magnetostrictive transducers are employed as sensors and actuators can be found in [8, 16]).

To fully utilize their capabilities as either sensors or actuators, the input and output characteristics of magnetostrictive materials must be quantified in a manner amenable to parameter estimation and control applications. As detailed in the literature (e.g., see [17, 19]) and outlined in the next section, the input/output characteristics of magnetostrictive materials are inherently nonlinear and display significant hysteresis. To utilize the transducer responses in a range useful for full control applications, accurate mathematical characterization of the nonlinearities and hysteresis is required.

The general techniques we use here to characterize the magnetic nonlinearities and hysteresis are based on Preisach-type operators. The use of Preisach techniques for characterizing general magnetic hysteresis is well-established in the literature (see [1, 6, 13, 15, 23, 24, 26] and references therein) and some aspects have been extended to magnetostrictives [2, 9]. In [2], the classical Preisach model was modified for Terfenol-D materials by considering a characterization for the output strain in terms of two inputs and two Preisach kernels. This was motivated by the observation that magnetostrictive materials exhibit hysteresis with respect to both magnetic field and stress. Further coupling between the kernels and input was included in the model proposed in [9].

In this work, we consider the modeling of nonlinearities and hysteresis in magnetostrictive transducers in the context of the generalized Preisach or Krasnoselskii-Pokrovskii kernels developed in [6]. Such generalizations of the classical Preisach theory are motivated by the goal of attaining a kernel which is continuous with respect to both time and shape parameters (as proven in [6], the classical Preisach kernel is discontinuous in both aspects). This provides a framework in which to prove well-posedness of models which incorporate magnetostrictive transducers. Furthermore, it yields a framework which is natural for the development of approximation techniques for both simulations and parameter estimation.

It should be noted that the modeling of nonlinearities and hysteresis through Preisach techniques is phenomenological rather than physics-based. It provides a mathematical characterization of the input/output relationships for magnetostrictive materials in lieu of a complete theory for the electromagnetic and magnetomechanical properties of the materials. As the physical theory is advanced, physics-based models may provide additional insights regarding the actuator/sensor mechanisms and hence replace the Preisach models. For example, theory based upon magnetic domain wall motion, which is used in [21, 22] to model hysteresis in ferromagnetic materials, may be applicable to magnetostrictive materials. At the current time,

however, several physical mechanisms in magnetostrictive materials are still not well understood, thus motivating the phenomenological or empirical characterization of the material.

The construction of magnetostrictive transducers and physical properties of the magnetostrictive materials are described in Section 2. The source and form of the nonlinearities and hysteresis are detailed to illustrate issues to be addressed in the models. The generalized Preisach kernels and operators developed in [6] are summarized in Section 3. In Section 4, a thick cantilever beam with magnetostrictive actuators is used as a prototype for structural models which incorporate magnetostrictive inputs. Modified Timoshenko equations are used to model the beam dynamics while generalized Preisach or Krasnoselskii-Pokrovskii operators are used to characterize the inputs. The well-posedness of the model and parameter estimation problem is established using the framework of [4, 6]. Although the framework is described here in the context of a specific, simple structure, it is sufficiently general to include structures comprised of plates and shells as well as structures in which nonlinear dynamics are significant.

2 Magnetostrictive Transducers

To illustrate issues which must be addressed when modeling magnetostrictive materials, the transducer depicted in Figure 1 is considered. This transducer is typical of those currently employed in applications and contains the basic components required for experimental use as a control actuator. Details regarding the construction and performance of this transducer can be found in [17].

The primary components of the transducer consist of a magnetostrictive rod, a wound wire solenoid, and a cylindrical permanent magnet. In current transducers, the magnetostrictive material is typically composed of terbium and dysprosium alloyed with iron. A commonly employed material is Terfenol-D (Ter: terbium, fe: iron, nol: Naval Ordinance Laboratory, D: dysprosium) which is constructed as a cylindrical rod and placed in the center of the transducer. The sensor/actuator capabilities of the material are due to the rotation of magnetic moments within the rod in the presence of an applied magnetic field. In ferromagnetic materials such as Terfenol-D, moments are ordered and exhibit a high degree of alignment at temperatures below the Curie point (regions in which moments are highly aligned are termed domains). As depicted in Figure 2a, the moments within domains are primarily oriented perpendicular to the longitudinal rod in the absence of an applied field. Prestressing the rod with the spring washer serves to increase the number of moments perpendicular to the axis (see Figure 2b) and places the material in compression. This latter objective is necessary due to the inherent brittleness of Terfenol-D. In the presence of a magnetic filed, the moments rotate so as to align with the field. Consequently, if the field is applied in the direction of the rod axis, the moments rotate in the sense depicted in Figure 2c and significant strains are generated. This is termed the Joule effect and provides the actuator capabilities of the transducer. Sensing is accomplished through the measurement of the magnetic fields which result when mechanical stresses cause rotations of the moments within domains (Villari effect). Details regarding these effects can be found in [19, 25].

The strains generated through an applied field are always positive since rotation of the moments from the prestressed perpendicular state leads to an increase in the rod length. As

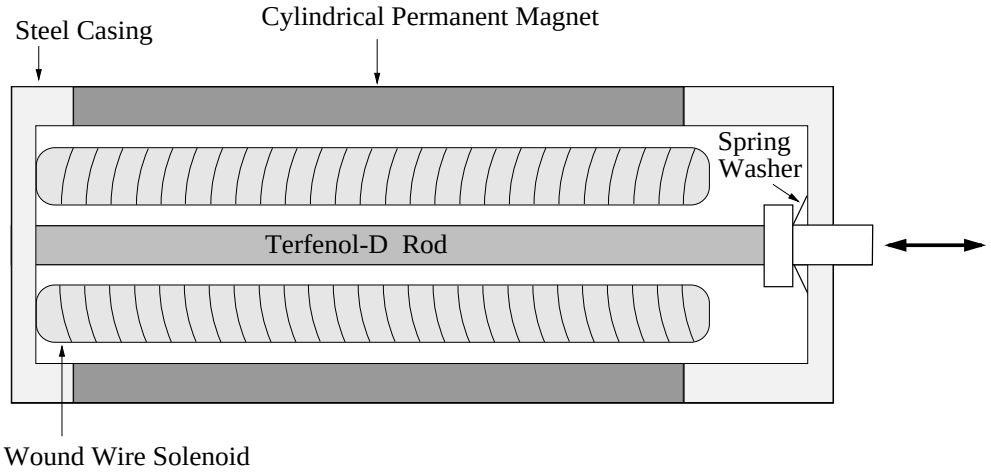

Figure 1. Cross section of a typical Terfenol-D magnetostrictive transducer.

indicated in Figure 3, the relationship between the applied magnetic flux or induction B and strain e is also highly nonlinear with saturation occurring at large field strengths. Moreover, slight hysteresis also exists between B and e at high drive levels (this is not depicted in the figure).

The generation of bidirectional strains is accomplished through either a DC current I_0 applied to the solenoid which surrounds the rod, or an enclosing cylindrical permanent magnet which provides a biasing magnetic induction B_0. A time varying current $I(t)$ is then used to vary the induction in the rod between 0 and B_m. This provides the capability of generating both positive and negative strains.

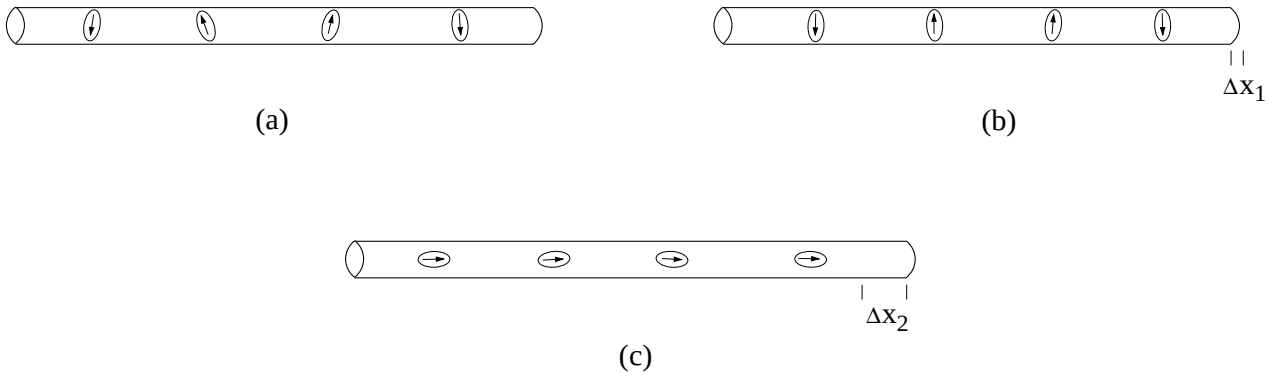

Figure 2. Magnetic domains in the Terfenol-D rod; (a) Orientation of moments within domains in unstressed rod with no applied field; (b) Orientation of moments in prestressed rod with no applied field; (c) Orientation of moments in prestressed rod when field is applied in direction of longitudinal rod axis.

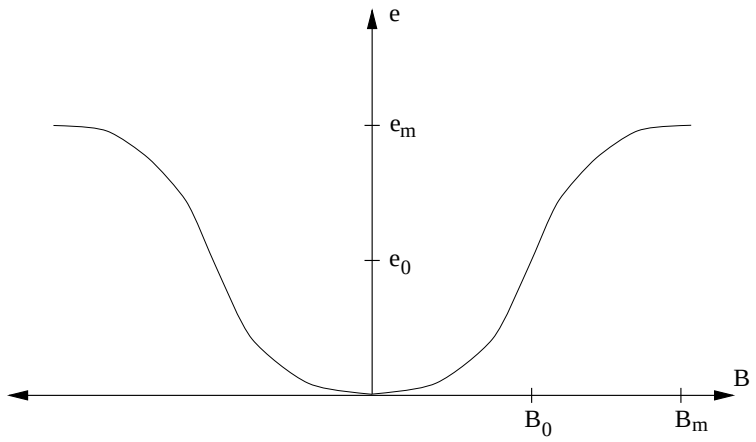

Figure 3. Strain distribution e generated by an applied magnetic induction B.

To model the transducer for actuator and sensor purposes, it is necessary to characterize the relationship between the current I applied to the solenoid, the resulting magnetic field H, the associated magnetic induction B and finally, the generated strains e. Furthermore, the quantification must incorporate the contributions due to the permanent magnet.

As detailed in [19], the magnetic induction and field are related by the permeability μ which is defined as

$$\mu = \frac{B}{H} .$$

The magnetic field is due both to the solenoid and the permanent magnet. The magnetic induction from the permanent magnet is approximated by $B_0 = \mu H_0$ while Ampère's law yields $B = \mu n I$, where n is the number of turns per unit length in the solenoid, as the approximate magnetic induction due to the solenoid (these are approximate since edge effects, air gaps, etc., are neglected).

For Terfenol-D, the permeability μ is highly nonlinear and exhibits significant hysteresis as indicated by the induction/field relations depicted in Figure 4a. As discussed in [2], this hysteresis is manifested with respect to both the applied magnetic field and stresses within the magnetostrictive material. To indicate the latter contribution, the permeability in magnetostrictive applications is often denoted by μ^σ. The hysteretic relationship between the magnetic field, magnetic induction and material stress are then inherently manifested in the field-strain relations as shown in Figure 4b.

As indicated by the preceding discussion, the nonlinear relationships between the applied current and magnetic induction are augmented by nonlinearities in the behavior of the magnetostrictive materials. For example, experimental results in [11, 14] indicate that the Young's modulus E^H for Terfenol is dependent upon the applied magnetic field which partially accounts for the dependence of magnetic hysteresis on the material stress. Furthermore, experimental results in [11, 14] demonstrate that other material properties such as magnetomechanical coupling coefficients are highly sensitive to operating conditions such as prestress level, AC drive levels, operating frequencies and temperature. To provide a framework amenable to characterization of these relationships, we summarize next necessary theory regarding generalized Preisach operators. The application of this theory to magnetostrictive materials in a structural setting is considered in the final section.

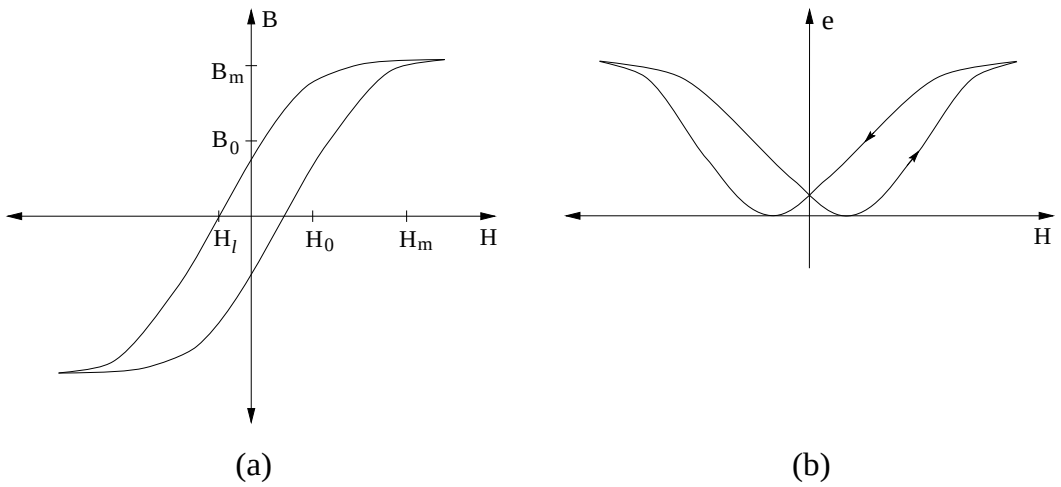

Figure 4. (a) Relationship between the magnetic field strength H and the magnetic flux density B; (b) Applied magnetic field H and resulting strain distribution e.

3 Preisach and Krasnoselskii-Pokrovskii Operators

In this section, we provide basic theory regarding Preisach-type operators in a Hilbert space setting. Classical Preisach kernels and operators are defined first and are then extended to kernels of Krasnoselskii-Pokrovskii type to attain desired continuity properties. The material in this section summarizes theory from [6, 7], and the reader is referred to those references for further details.

To motivate the general kernels used later, we first illustrate with a single delayed, relay operator $\hat{k}$. This kernel is characterized in terms of crossing times $\tau(t)$ defined by

$$\tau(t) = \{\eta \in (0,T] \,|\, u(\eta) = s_1 \text{ or } u(\eta) = s_2\}$$

where $s = (s_1, s_2)$ are points in the Preisach half plane

$$\mathcal{S} = \left\{ s \in \mathbb{R}^2 \,|\, s = (s_1, s_2), s_1 < s_2 \right\}$$

and u denotes an input function. The values s_1, s_2 are threshold values for the multivalued kernel as reflected in the definition

$$[\hat{k}_s(u,\xi)](t) = \begin{cases} [\hat{k}_s(u,\xi)](0) & \text{if} \quad \tau(t) = \emptyset \\ -1 & \text{if} \quad \tau(t) \neq \emptyset \text{ and } u(\max \tau(t)) = s_1 \\ +1 & \text{if} \quad \tau(t) \neq \emptyset \text{ and } u(\max \tau(t)) = s_2 \,. \end{cases}$$

A depiction of this kernel is given in Figure 5. The starting value

$$[\hat{k}_s(u,\xi)](0) = \begin{cases} -1 & \text{if} \quad u(0) \leq s_1 \\ \xi & \text{if} \quad s_1 < u(0) < s_2 \\ +1 & \text{if} \quad u(0) \geq s_2 \end{cases}$$

defines the initial state of the kernel in terms of the parameter $\xi \in \{-1, 1\}$.

The output remains on a branch until a threshold is reached in the monotonically increasing input u. At that point, the output jumps to the other saturation value and remains there until the other threshold value is reached. For example, an output response starting with a value of -1 will retain that value until $u(t)$ reaches s_2. The output then jumps to $+1$ until the threshold value of s_1 is reached.

The classical Preisach operators are then defined in terms of parallel collections of these single relay operators. To this end, we let $\mathcal{M}$ denote the set of all finite, signed Borel measures on $\mathcal{S}$ and let f be a Borel measurable function mapping $\mathcal{S} \to \{-1, 1\}$. For $u \in C[0, T]$ and $\nu \in \mathcal{M}$, the Preisach operator is defined by

$$[\hat{P}_\nu(u, f)](t) = \int_{\mathcal{S}} [\hat{k}_s(u, f(s))](t) d\nu(s).$$

The goal in the parameter identification problem is to estimate the measure ν so that the model response "fits" experimental data in a least squares sense.

While this provides an operator which is useful for many applications, this classical definition does not yield a kernel, and hence operator, which is continuous with respect to either time or parameters. Specifically, as proven in [6], the mapping in time

$$t \mapsto [\hat{k}_s(u, \xi)](t)$$

and the parameter space mapping

$$s \mapsto [\hat{k}_s(u, \xi)](t)$$

are discontinuous for the classical Preisach kernel $\hat{k}_s(u, \xi)$. Continuity in time is important from a physical perspective while continuous parameter dependence is crucial for the development of practical parameter estimation methods.

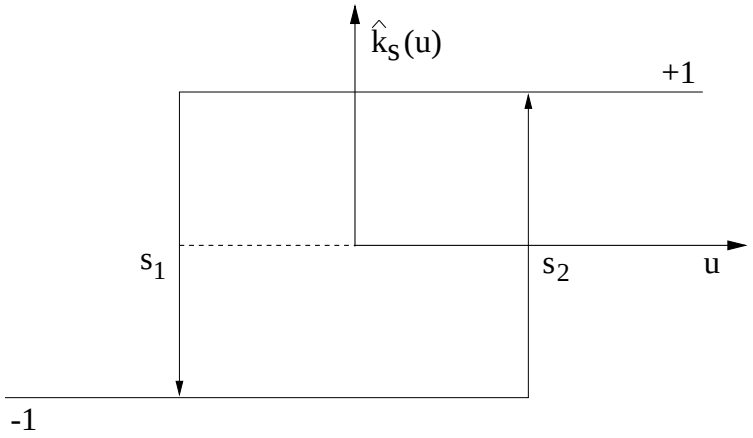

Figure 5. Single Preisach relay operator with threshold values s_1, s_2.

To avoid the difficulties associated with the discontinuous mappings, a Krasnoselskii-Pokrovskii kernel of the type discussed in [6] is employed. This kernel is somewhat less general than the influence operators considered in [23] and arises as an extension of smoothed Preisach operators. These operators differ from the previously-defined Preisach operator in the manner through which an envelope of admissible paths is defined. In this case, an envelope is provided by translates

$$r_{s_1} = r(x - s_1)$$
$$r_{s_2} = r(x - s_2)$$

of a Lipschitz continuous ridge function $r(x)$ as depicted in Figure 6. For monotone inputs $u_m \in C[0,T]$, a monotone output operator is defined by

$$[\mathcal{R}(u_m, \xi)](t) = \begin{cases} \max\{\xi, r(u_m(t) - s_2)\} & \text{if } u_m \text{ is non-decreasing} \\ \min\{\xi, r(u_m(t) - s_1)\} & \text{if } u_m \text{ is non-increasing}\,. \end{cases}$$

In terms of this operator, a kernel is defined for piecewise monotone inputs $u_{pm} \in C[0,T] \cap S_{1,j}[0,T]$, where $S_{1,j}[0,T]$ is the set of piecewise linear splines with j knots in $[0,T]$, in the following manner. The initial value of the operator is taken to be $\mathcal{R}_0 = \xi$. A kernel k_s is then defined recursively on each subinterval by

$$[k_s(u_{pm}, \xi)](t) = [\mathcal{R}(u_{pm}, \mathcal{R}_{k-1})](t)\ ,\ t \in [t_{k-1}, t_k] \tag{3.1}$$

where $\mathcal{R}_k \equiv \mathcal{R}(u_{pm}, \mathcal{R}_{k-1})(t_k)$, $k = 1, \cdots, j$. The input and action of this kernel are illustrated in Figure 7. This provides a definition of the kernel useful for computational algorithms in which inputs are discretized in terms of a piecewise linear basis. This definition is readily extended to arbitrary $u \in C[0,T]$ through standard density arguments as detailed in [23].

It is natural in the applications considered here to formulate the hysteretic input operator in a manner commensurate with a weak model formulation. We thus consider a space of test functions V and state space H in which V is continuously and densely embedded in H and forms a Gelfand triple

$$V \hookrightarrow H \simeq H^* \hookrightarrow V^*.$$

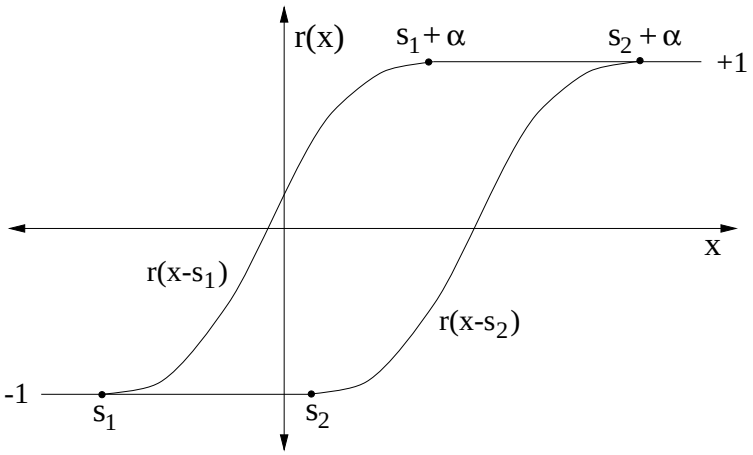

Figure 6. Hysteresis envelope provided by the translates r_1 and r_2 of the ridge function $r(x)$.

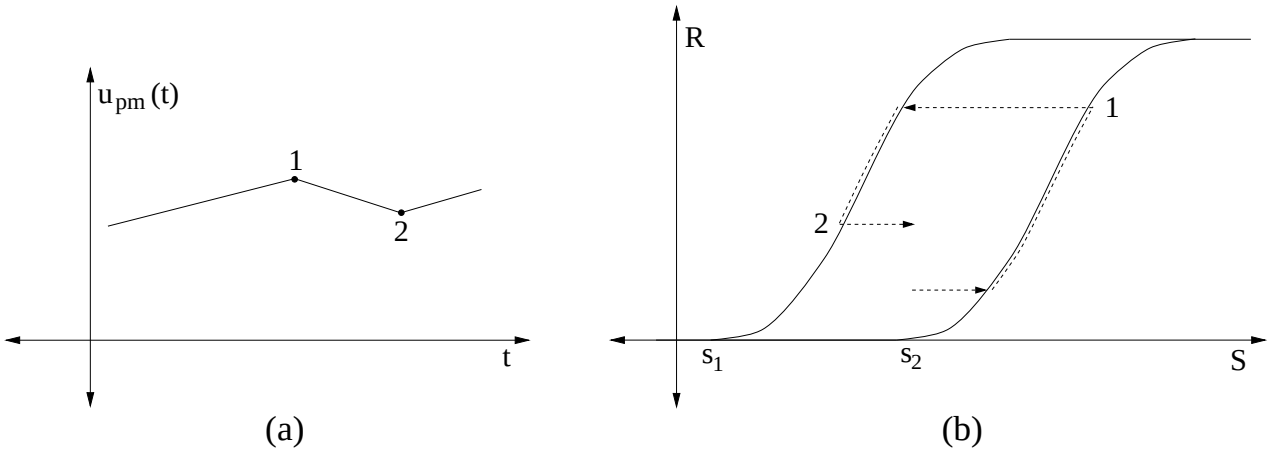

Figure 7. (a) Piecewise monotone input; (b) Output from the Krasnoselskii-Pokrovskii kernel in response to a piecewise monotone input.

The following theorem from [6] summarizes the continuity properties of the kernel k_s and quantifies the resulting input operator $\mathcal{B}_\nu$.

Theorem 1. Let k_s denote the kernel defined in (3.1) and let $\bar{\mathcal{S}}$ denote the closure of $\mathcal{S}$ in $\mathbb{R}^2$.

(1) For each $s \in \bar{\mathcal{S}}$ and $\xi \in \{-1, 1\}$, the kernel satisfies $k_s(\cdot, \xi) : C[0,T] \to C[0,T]$.

(2) For each $u \in C[0,T], \xi \in \{-1,1\}$ and $t \in C[0,T]$, the map $s \mapsto [k_s(u,\xi)](t)$ is continuous from $\bar{\mathcal{S}}$ to $\mathbb{R}$.

(3) For $g \in V^*$ and $\nu \in \mathcal{M}$, the control influence operator B_ν defined by

$$[B_\nu(u,\xi)](t) \equiv g\,[P_\nu(u,\xi)](t) \equiv g \int_{\bar{\mathcal{S}}} [k_s(u,\xi)](t)\, d\nu(s) \tag{3.2}$$

satisfies $B_\nu(u,\xi) \in L^2((0,T); V^*)$.

Remark 1. The kernel k_s and control influence operator B_ν defined in this manner can be readily incorporated in a framework for proving model well-posedness and the existence of a measure which minimizes an appropriate parameter estimation functional. Moreover, as illustrated in Figure 7, this kernel yields a technique for characterizing the nested hysteresis curves which are common in magnetostrictive applications.

4 Characterization of Hysteresis for Structural Models with Magnetostrictive Transducers

To illustrate the use of the operator framework described in the last section to characterize hysteresis in magnetostrictive materials, we consider the modeling of magnetostrictive transducers mounted to a thick cantilever beam as depicted in Figure 8. The transducers are considered to be mounted to the clamps at the fixed edge of the beam so that mass loading from the actuators themselves is minimized. A rigid bar is used connect the end of the

Figure 8. Cantilever beam with magnetostrictive actuators.

Terfenol-D rod in the transducer to the beam. By driving the transducers out-of-phase, bending moments are generated in a manner which can be used to attenuate beam vibrations. As described in [12], this experimental setup has been used in initial experiments to determine the potential of magnetostrictive transducers as structural actuators. Due to limitations in models and control laws, driving currents in the experiments were restricted to a range in which linearized results could be employed. Even in this restricted regime, the results of [12] demonstrate the utility of the magnetostrictive transducers for structural applications.

It should be noted that a beam is considered here both due to its previous experimental use and the relative simplicity of the resulting model. The operator techniques are quite general, however, and can be applied in a similar manner to structures comprised of plates or shells as well as structures undergoing large deformations which leads to nonlinear models (e.g., von Kármán models).

For modeling purposes, we take the beam to have length ℓ, width b and thickness h. The density, Young's modulus, Kelvin-Voigt damping coefficient and air damping coefficient for the beam are denoted by ρ_b, E_b, c_{D_b} and γ, respectively. The cross-sectional area of the Terfenol rod is denoted by A_{mag} while the Young's modulus and damping coefficient for the Terfenol rod are denoted by E^H c_D^H. The length and width of the connecting bar are denoted by ℓ_r and b_r, respectively, while the bar density is given by ρ_r.

4.1 Strong Form of Beam Model

The Timoshenko equations

$$\left.\begin{aligned} &\rho(x)\frac{\partial^2 w}{\partial t^2}(t,x) + \gamma\frac{\partial w}{\partial t}(t,x) - \frac{\partial Q}{\partial x}(t,x) = \tilde{f}(t,x) \\ &\rho r(x)\frac{\partial^2 \alpha}{\partial t^2}(t,x) - \frac{\partial M}{\partial x}(t,x) + Q(t,x) = -\frac{\partial M_{mag}}{\partial x}(t,x) \end{aligned}\right\} \quad , \quad 0 < x < \ell \ , \ t > 0$$
$$\left.\begin{aligned} &w(t,0) = \alpha(t,0) = 0 \\ &M(t,\ell) = Q(t,\ell) = 0 \end{aligned}\right\} \quad , \quad t > 0 \tag{4.1}$$

where w and α denote the transverse displacement and cross-sectional rotation, respectively, are used to model the beam dynamics. Exogenous surface forces to the beam are denoted by

$\tilde{f}(t,x)$ while $\rho(x)$ is the composite density of the structure. The cross-sectional area of the beam is given by $A(x)$, while $r(x) \equiv I(x)/A(x)$ where $I(x)$ is the moment of inertia of the cross-sectional area. Note that these quantities are spatially variable due to the nonhomogeneity in the region of the connection rod. Finally, the internal bending moment and shear force are given by $M(t,x)$ and $Q(t,x)$, respectively, while the external bending moment generated by the magnetostrictive actuators is denoted by $M_{mag}(t,x)$.

To determine appropriate functional forms for the density, internal moment and shear force, the structural contributions due to the connecting bar and Terfenol rod must be quantified. We assume here that the connecting bars are perfectly rigid and contribute mass to the beam but do not affect the bending moments (we neglect air resistance to the bars). The actuator and Terfenol rod are considered to be supported from the boundary clamps so they do not contribute mass to the beam. The Terfenol rod is assumed to contribute an elastic stress which is uniform across the cross-sectional area of the rod.

Under the assumption of uniform cross-sectional strains in the magnetostrictive rods, the density, stiffness and Kelvin-Voigt damping parameters for the structure are then taken to be

$$\begin{aligned} \rho(x) &= \rho_b hb + 2\rho_r b_r \ell_r \chi_{rod}(x) \\ EI(x) &= \frac{E_b h^3 b}{12} + 2A_{mag} E^H \left(h/2 + \ell_r\right)^2 \chi_{rod}(x) \\ c_D I(x) &= \frac{c_{D_b} h^3 b}{12} + 2A_{mag} c_D^H \left(h/2 + \ell_r\right)^2 \chi_{rod}(x) \end{aligned} \tag{4.2}$$

where the location of the rods is delineated by the characteristic function χ_{rod} which has a value of 1 in the region covered by the connection bar and is 0 elsewhere. The internal moment and shear are then given by

$$\begin{aligned} M(t,x) &= EI(x)\frac{\partial \alpha}{\partial x}(t,x) + c_D I(x)\frac{\partial^2 \alpha}{\partial x \partial t}(t,x) \\ Q(t,x) &= \kappa AG(x)\beta(t,x) + \kappa A c_Q(x)\frac{\partial \beta}{\partial t}(t,x) \end{aligned} \tag{4.3}$$

where κ is a correction factor which accounts for the fact that the outer surface of the beam cannot support a shear stress, $G(x)$ is the shear modulus and $c_Q(x)$ represents resistance to the shear strain rate. Finally, the shear deformations are defined by

$$\beta(t,x) = \frac{\partial w}{\partial x}(t,x) + \alpha(t,x)\,.$$

It should be noted that the contributions due to the connection rods are dependent upon the exact experimental setup and different assumptions and models can also be used to incorporate the passive rod contributions. In all cases, the piecewise constant parameters $\rho(x), r(x), EI(x), G(x), c_D I(x), c_Q(x)$ and constant parameter γ must be estimated through a least squares fit to experimental data to attain a reasonable model for the specific experimental device (The values determined by (4.2) cannot be used with certainty when modeling the experimental apparatus due to inaccuracies in manufacturer specifications, etc.; however,

they can be used as initial values for the optimization routine.) Note that in the moment and shear expressions (4.3) and equations (4.1), parameters have been combined to yield a single value to be estimated.

To characterize the external moment generated by the magnetostrictive transducers, we will assume that an offset DC current I_0 is used to provide the magnetic field bias necessary to attain bidirectional strains. Ampère's law then yields the magnetic induction

$$B(t) = \mu^\sigma n[I(t) + I_0] \tag{4.4}$$

where again, n is the number of terms per unit length in the solenoid, $I(t)$ is the current applied to the solenoid, and μ^σ is the permeability. As noted in Section 2, the permeability exhibits both stress-dependent nonlinearities and hysteresis due to the magnetic field.

The strain can be related to the magnetic induction through the nonlinear equation

$$e(t) = \mathcal{K}_B B(t) \tag{4.5}$$

where $\mathcal{K}_B$ depends upon the magnetic induction B. Moreover, the external stress-strain relation

$$\sigma(t) = E^H e(t) \tag{4.6}$$

is also nonlinear since the Young's modulus E^H for the Terfenol-D rod can be highly dependent upon the applied magnetic field. Finally, the external moment generated by the Terfenol-D rod is

$$M_{mag}(t,x) = 2A_{mag}(\ell_r + h/2)\sigma(t)\chi_{rod}(x) \tag{4.7}$$

where ℓ_r denotes the length of the connection bar and A_{mag} is the cross-sectional area of the Terfenol rod.

Combination of (4.7) with (4.4)-(4.6) will yield a relationship for the external moment in terms of the applied current $I(t)$. However, this relationship is not directly useful for modeling transducer dynamics since the parameters $\mu^\sigma, \mathcal{K}_B$ and E^H are highly nonlinear and exhibit significant hysteresis.

An alternative is to characterize the external moment through the fitting of hysteresis and material nonlinearities in terms of the Preisach kernels described in Section 3. Specifically, the external moment generated by the magnetostrictive transducer can be described by the relation

$$M_{mag}(t,x) = 2A_{mag}(\ell_r + h/2)[P_\nu(I,\xi)](t)\chi_{rod}(x) \tag{4.8}$$

where

$$[P_\nu(I,\xi)](t) \equiv \int_{\mathcal{S}} [k_s(I,\xi)](t)\, d\nu(s)\,. \tag{4.9}$$

The kernel k_s is the extension of that defined in (3.1) to $I \in C[0,T]$. In essence, the method characterizes the hysteresis and material nonlinearities through curve fitting in terms of a measure ν which, for a given set of experimental operating conditions, is estimated through a least squares fit to data. Due to its generality, the technique can be used to characterize a wide variety of transducer responses. Furthermore, the technique provides a framework suitable for parameter estimation and subsequent controller design.

4.2 Weak Form of Beam Model

As noted when (4.3) and (4.8) are employed in (4.1), the use of the strong form of the beam model leads to the differentiation of discontinuous material parameters and inputs. It also necessitates the use of high-order approximating elements. To alleviate these difficulties and provide a framework amenable to analysis and approximation, we consider a corresponding weak form of the model.

For this system, the state is taken to be $y = (w, \alpha)$ in the Hilbert space $H = L^2(0,\ell) \times L^2(0,\ell)$ with the inner product

$$\langle \Phi, \Psi \rangle_H = \int_0^\ell \rho\phi_1\psi_1\, dx + \int_0^\ell \rho r\phi_2\psi_2\, dx$$

where $\Phi = (\phi_1, \phi_2), \Psi = (\psi_1, \psi_2)$. The space of test functions is $V = H_L^1(0,\ell) \times H_L^1(0,\ell)$, $H_L^1(0,\ell) \equiv \{\phi \in H^1(0,\ell) \mid \phi(0) = 0\}$, with the inner product

$$\langle \Phi, \Psi \rangle_V = \int_0^\ell (\phi_1' + \phi_2)(\psi_1' + \psi_2)\, dx + \int_0^\ell \phi_2'\psi_2'\, dx\,.$$

It should be noted that with these choices, V is continuously and densely embedded in H and that V and H form a Gelfand triple; that is

$$V \hookrightarrow H \simeq H^* \hookrightarrow V^*\,.$$

A weak form of the modeling equations is then

$$\begin{aligned} &\int_0^\ell \rho\ddot{w}\psi_1\, dx + \int_0^\ell \gamma\dot{w}\psi_1\, dx + \int_0^\ell Q\psi_1'\, dx + \int_0^\ell \rho r\ddot{\alpha}\psi_2\, dx + \int_0^\ell M\psi_2'\, dx + \int_0^\ell Q\psi_2\, dx \\ &\quad = \int_0^\ell M_{mag}\psi_2'\, dx + \int_0^\ell \tilde{f}\psi_1\, dx \end{aligned} \tag{4.10}$$

for all $\Psi = (\psi_1, \psi_2) \in V$. In this form, derivatives are transferred onto suitably smooth test functions. This alleviates the difficulties associated with the discontinuities and reduces smoothness requirements on approximate solutions.

4.3 Model Well-Posedness

To provide a framework amenable to proving the well-posedness of the model and parameter estimation problem, it is advantageous to formulate the model in terms of sesquilinear forms and the operators which they generate. To this end, recall that $y(t) = (w(t,\cdot), \alpha(t,\cdot))$ and define

$$\begin{aligned} \sigma_1(q)(y(t),\Psi) &= \int_0^\ell EI\alpha'\psi_2'\, dx + \int_0^\ell \kappa AG(w' + \alpha)(\psi_1' + \psi_2)\, dx \\ \sigma_2(q)(y(t),\Psi) &= \int_0^\ell c_D I\alpha'\psi_2'\, dx + \int_0^\ell \kappa Ac_Q(w' + \alpha)(\psi_1' + \psi_2)\, dx + \int_0^\ell \gamma w\psi_1\, dx \end{aligned} \tag{4.11}$$

where $q = (\rho, r, EI, G, c_D I, c_Q, \gamma)$ is considered in an admissible parameter space $\mathcal{Q}$. It can be directly verified that σ_1 and σ_2 satisfy the boundedness and ellipticity conditions

$$\text{(H1)} \qquad |\sigma_1(q)(\Phi,\Psi)| \le c_1 |\Phi|_V |\Psi|_V \ , \ c_1 \in \mathbb{R}$$

$$\text{(H2)} \qquad \mathrm{Re}\,\sigma_1(q)(\Phi,\Phi) \ge c_2 |\Phi|_V^2 \ , \ c_2 > 0$$

$$\text{(H3)} \qquad |\sigma_2(q)(\Phi,\Psi)| \le c_3 |\Phi|_V |\Psi|_V \ , \ c_3 \in \mathbb{R}$$

$$\text{(H4)} \qquad \mathrm{Re}\,\sigma_2(q)(\Phi,\Phi) + c_4 |\Phi|_H^2 \ge c_5 |\Phi|_V^2 \ , \ c_4 \in \mathbb{R}, c_5 > 0$$

for all $\Phi, \Psi \in V$ where the constants $c_1, \cdots, c_5$ are independent of the parameters $q \in \mathcal{Q}$.

From (4.8), it follows that the transducer contributions can be represented in terms of the operator $B_\nu : U \to V^*$ by

$$\begin{aligned} \langle [B_\nu(u,\xi)](t), \Psi \rangle_{V^*,V} &= \langle [P_\nu(u,\xi)](t) g, \Psi \rangle_{V^*,V} \\ &\equiv [P_\nu(u,\xi)](t) \int_0^\ell 2A_{mag}(\ell_r + h/2)\psi_2' \chi_{rod}\, dx \end{aligned}$$

where $U = \mathbb{R}$, $\langle \cdot, \cdot \rangle_{V^*,V}$ is the usual duality product and P_ν is defined in (4.9). Note that from Theorem 1, it follows that $B_\nu(u,\xi) \in L^2((0,T);V^*)$. Finally, with the definition $f(t) = (\rho^{-1}\tilde{f}(t,\cdot), 0)$, we can write the weak form (4.10) in the abstract variational form

$$\begin{aligned} &\langle \ddot{y}(t), \Psi \rangle_{V^*,V} + \sigma_2(q)(\dot{y}(t), \Psi) + \sigma_1(q)(y(t), \Psi) = \langle [B_\nu(u,\xi)](t) + f(t), \Psi \rangle_{V^*,V} \\ &y(0) = y_0 \quad , \quad \dot{y}(0) = y_1 \end{aligned} \tag{4.12}$$

for all $\Psi \in V$.

An equivalent system can be obtained by invoking the boundedness of σ_1, σ_2 to define operators $A_i(q) \in \mathcal{L}(V, V^*)$, $i = 1, 2$, by

$$\begin{aligned} \langle A_1\Phi, \Psi \rangle_{V^*,V} &= \sigma_1(q)(\Phi,\Psi) \\ \langle A_2\Phi, \Psi \rangle_{V^*,V} &= \sigma_2(q)(\Phi,\Psi) \end{aligned} \quad , \quad \Phi, \Psi \in V \, .$$

In operator form, the equations governing the beam dynamics then have the form

$$\ddot{y}(t) + A_2(q)\dot{y}(t) + A_1(q)y(t) = [B_\nu(u,\xi)](t) + f(t) \tag{4.13}$$

in V^*.

The subsequent result concerning the existence, uniqueness and regularity of solutions follows directly from Theorem 2.1 and Remark 2.1 of [4].

Theorem 2. Let $\mathcal{Q}$ denote a compact metric space and $\mathcal{M}$ denote the set of finite, signed Borel measures on $\mathcal{S}$. Consider inputs $u \in C[0,T]$ and $f \in \mathcal{B}(\mathcal{S}, \{-1,1\})$. Finally, let σ_1, σ_2 be given by (4.11) and hence satisfy (H1)-(H4). For each $(q,\nu) \in \mathcal{Q} \times \mathcal{M}$, there then exists a unique solution y to (4.12) which satisfies

$$\begin{aligned} y &\in C((0,T);V) \subset L^2((0,T);V) \\ \dot{y} &\in C((0,T);H) \cap L^2((0,T);V) \\ \ddot{y} &\in L^2((0,T);V^*) \, . \end{aligned}$$

Remark 2. As noted in Remark 4.2 of [8], the regularity results in Theorem 2 can actually be strengthened to yield

$$y \in C((0,T);V)$$
$$\dot{y} \in C((0,T);H)\,.$$

4.4 Parameter Estimation

The goal in the parameter estimation problem is to determine material parameters $q = (\rho, r, EI, G, c_D I, c_Q, \gamma)$ and a measure ν given data measurements $\hat{z}$ from some observable subspace $\mathcal{Z}$ of the state space. The form of the quadratic functional to be minimized depends on the experimental data which is available. For time domain data consisting of position, velocity or acceleration measurements at points $\bar{x}$ on the beam, an appropriate functional is

$$J(q,\nu) = \sum_i \left| \frac{\partial^s y}{\partial t^s}(t_i, \bar{x}; q, \nu) - \hat{z}_i \right|^2 \tag{4.14}$$

with $s = 0, 1$ or 2. Other functionals incorporating either time or frequency domain data can be found in [8]. In each case, the minimization is performed subject to y satisfying (4.12) for $q \in \mathcal{Q}$ and $\nu \in \mathcal{A} \subset \mathcal{M}$ where $\mathcal{A}$ is an appropriate class of measures.

As noted previously, the parameters $\rho, r, EI, G, c_D I, c_Q$ are assumed to be piecewise constant with partition points at the connection rod edges. The air constant γ is constant, and all seven parameters are positive. The admissible parameter space $\mathcal{Q}$ is then taken to be a compact subset of the metric space $\tilde{\mathcal{Q}} = [L^\infty(0,\ell)]^6 \times \mathbb{R}$ with elements piecewise constant between partition points and satisfying the positivity constraints.

An appropriate choice for $\mathcal{A}$ is a set of probability measures with a metric which yields convergence in distribution. Specifically, let $\mathcal{S}_\Delta$ be a compact subset of $\bar{\mathcal{S}}$ and let $\mathcal{P}(\mathcal{S}_\Delta)$ denote the set of Borel probability measures ν on $\mathcal{S}_\Delta$. The space $\mathcal{A}$ is then defined to be $\mathcal{P}(\mathcal{S}_\Delta)$ endowed with the Prohorov metric which is defined for $\nu_1, \nu_2 \in \mathcal{P}(\mathcal{S}_\Delta)$ by

$$\rho(\nu_1,\nu_2) = \inf\{\varepsilon > 0 \,|\, \nu_1(F) \le \nu_2(F^\varepsilon) + \varepsilon,\ F \text{ closed},\ F \subset \mathcal{S}_\Delta\}$$

(see [10] for details regarding this metric). Here F^ε denotes an ε neighborhood for F.

Remark 3. As detailed in [3, 6, 7, 10], the space $\mathcal{A}$ satisfies the following properties.

(a) Let $C(\mathcal{S}_\Delta)$ denote the space of continuous functions on $\mathcal{S}_\Delta$. Since $\mathcal{P}(\mathcal{S}_\Delta) \subset [C(\mathcal{S}_\Delta)]^*$, convergence in the Prohorov metric is equivalent to weak* convergence; that is

$$\nu_k \to \nu \iff \int_{\mathcal{S}_\Delta} f d\nu_k \to \int_{\mathcal{S}_\Delta} f d\nu$$

for $f \in C(\mathcal{S}_\Delta)$.

(b) $\mathcal{A}$ is a compact metric space.

(c) Consider the control influence operator B_ν defined in (3.2) and let $y(q,\nu)$ be a solution to (4.12). For the functional $J(q,\nu)$ defined in (4.14) with fixed $q \in Q$, the map $\nu \to J(q,\nu)$ is weak* lower semicontinuous from $\mathcal{P}(\mathcal{S}_\Delta)$ to $\mathbb{R}$.

The following theorem taken from [6] specifies conditions under which the parameter estimation problem with the magnetostrictive material inputs is well-posed. When combined with theory from [5], it provides a framework for numerically estimating physical and hysteresis shape parameters through a least squares fit to experimental data.

Theorem 3. Let B_ν denote the magnetostrictive input operator defined in (3.2) and $y(q,\nu)$ be the solution to (4.12). If $\mathcal{S}_\Delta$ is a compact subset of $\bar{\mathcal{S}}$, then there is a probability measure $\nu_0 \in \mathcal{P}(\mathcal{S}_\Delta)$ which solves the minimization problem

$$J(q,\nu_0) = \inf_{\nu \in \mathcal{P}(\mathcal{S}_\Delta)} J(q,\nu)$$

for the functional $J(q,\nu)$ defined in (4.14).

5 Concluding Remarks

This paper addresses the characterization of material nonlinearities and hysteresis inherent to magnetostrictive materials at middle to high range drive levels. The hysteresis is induced by both magnetic fields and stresses within the material while additional nonlinearities arise in the strain-magnetic induction relations and stress-strain relations. Some of the mechanisms leading to these nonlinear input/output relations have been modeled in terms of electromagnetic and magnetomechanical theories [20, 21, 22]. However, several mechanisms governing magnetostrictive properties are still not completely characterized by physics-based models. This motivates a mathematical characterization in terms of phenomenological Preisach techniques.

Preisach models are empirical in the sense that they can be used to mathematically represent hysteresis curves in terms of shape parameters determined through least squares fits to experimental data. Since the models are not directly derived from the physics of the system, they can be used to model dynamics in which the underlying physics is not thoroughly understood. The price paid for this generality is the loss of insight which can sometimes be provided by a physic-based model.

In this work, Krasnoselskii-Pokrovskii kernels are used to characterize magnetostrictive inputs to a flexible structure. As detailed in [6], such kernels are advantageous over classical Preisach kernels due to the property that they are continuous with respect to both time and shape parameters. The operators generated via these kernels are then used to formulate the models in a Hilbert space framework. Well-posedness of the models is obtained through the theory of [4] while existence of optimal physical parameters and an optimal measure for characterizing the hysteresis curve follows from the theory of [3, 5, 6]. Hence for structural systems with magnetostrictive transducers, this characterization technique provides a model which is amenable to analysis and approximation. In future investigations, the practical efficacy of this model will be tested through validation experiments.

Acknowledgements

The author thanks H.T. Banks, CRSC, North Carolina State University, for suggestions and input regarding the generalized Preisach techniques employed in this paper.

References

[1] A.A. Adly and I.D. Mayergoyz, "A New Vector Preisach-Type Model of Hysteresis," *Journal of Applied Physics*, 73(10), 1993, pp. 5824-5826.

[2] A.A. Adly, I.D. Mayergoyz and A. Bergqvist, "Preisach Modeling of Magnetostrictive Hysteresis," *Journal of Applied Physics*, 69(8), 1991, pp. 5777-5779.

[3] H.T. Banks and B.G. Fitzpatrick, "Estimation of Growth Rate Distributions in Size Structured Population Models," *Quarterly of Applied Mathematics*, 49, 1991, pp. 215-235.

[4] H.T. Banks, K. Ito and Y. Wang, "Well-Posedness for Damped Second Order Systems with Unbounded Input Operators," *Differential and Integral Equations*, 8, 1995, pp. 587-606.

[5] H.T. Banks and K. Kunisch, *Estimation Techniques for Distributed Parameter Systems*, Birkhäuser, Boston, 1989.

[6] H.T. Banks, A.J. Kurdilla and G. Webb, "Identification of Hysteretic Control Influence Operators Representing Smart Actuators; Part I: Formulation," CRSC Technical Report CRSC-TR96-14, April, 1996; *Mathematical Problems in Engineering*, submitted.

[7] H.T. Banks and A.J. Kurdilla, "Hysteretic Control Influence Operators Representing Smart Material Actuators: Identification and Control; CRSC Technical Report CRSC-TR96-23, August, 1996; Proceedings of the 35th IEEE Conference on Decision and Control, Kobe, Japan, December 1996, pp. 3711-3716.

[8] H.T. Banks, R.C. Smith and Y. Wang, *Smart Material Structures: Modeling, Estimation and Control*, Masson/John Wiley, Paris/Chichester, 1996.

[9] A. Bergqvist and G. Engdahl, "A Phenomenological Magnetomechanical Hysteresis Model," *Journal of Applied Physics*, 75(10), 1994, pp. 5496-5498.

[10] P. Billingsley, *Convergence of Probability Measures,* John Wiley, New York, 1968.

[11] F.T. Calkins and A.B. Flatau, "Transducer Based Measurement of Terfenol-D Material Properties," SPIE 1996 Proceedings on Smart Structures and Integrated Systems, Paper No. 67, Vol. 2717, February 1996.

[12] F.T. Calkins, R.L. Zrostlik and A.B. Flatau, "Terfenol-D Vibration Control of a Rotating Shaft," Proceedings of the 1994 ASME International Mechanical Engineering Congress and Exposition, Chicago IL; In *Adaptive Structures and Composite Materials Analysis and Applications* AD-Vol. 45, 1996, pp. 267-274.

[13] S.H. Charap and A. Ktena, "Vector Preisach Modeling," *Journal of Applied Physics*, 73(10), 1993, pp. 5818-5823.

[14] M.J. Dapino, F.T. Calkins, D.L. Hall and A.B. Flatau, "Measured Terfenol-D Material Properties Under Varied Operating Conditions," SPIE 1996 Proceedings on Smart Structures and Integrated Systems, Paper No. 66, Vol. 2717, February 1996.

[15] G. Friedman and D. Ahya, "Hybrid Boundary-Volume Galerkin's Method for Solution of Magnetostatic Problems with Hysteresis," *Journal of Applied Physics*, 73(10), 1993, pp. 5836-5838.

[16] M.V. Gandhi and B.S. Thompson, *Smart Materials and Structures*, Chapman and Hall, New York, 1992.

[17] D.L. Hall and A.B. Flatau, "Nonlinearities, Harmonics and Trends in Dynamic Applications of Terfenol-D," Proceedings of the SPIE Conference on Smart Structures and Intelligent Materials, Vol. 1917, Part 2, 1993, pp. 929-939.

[18] D.L. Hall and A.B. Flatau, "Broadband Performance of a Magnetostrictive Shaker," *Active Control of Noise and Vibration 1992*, DSC Volume 38, American Society of Mechanical Engineers, 1992, pp. 95-104.

[19] D.C. Jiles, *Introduction to Magnetism and Magnetic Materials*, Chapman and Hall, New York, 1991.

[20] D.C. Jiles, "Theory of the Magnetomechanical Effect," *Journal of Physics D: Applied Physics*, 28, 1995, pp. 1537-1546.

[21] D.C. Jiles and D.L. Atherton, "Theory of Ferromagnetic Hysteresis," *Journal of Magnetism and Magnetic Materials*, 61, 1986, pp. 48-60.

[22] D.C. Jiles, J.B. Thoelke and M.K. Devine, "Numerical Determination of Hysteresis Parameters for the Modeling of Magnetic Properties Using the Theory of Ferromagnetic Hysteresis," *IEEE Transactions on Magnetics*, 28(1), 1992, pp. 27-35.

[23] M. Krasnoselskii and A. Pokrovskii, *Systems with Hysteresis*, Springer, Berlin, 1989; Russian Edition, Nauka, Moscow, 1983.

[24] E.D. Torre "Energy Considerations in Hysteresis Models," *IEEE Transactions on Magnetics*, 28(5), 1992, pp. 2608-2610.

[25] E. du Trémolet de Lacheisserie, *Magnetostriction: Theory and Applications of Magnetoelasticity*, CRS Press, Ann Arbor, 1993.

[26] A. Visintin, *Differential Models of Hysteresis*, Springer-Verlag, New York, 1994.